RESEARCH PAPERS

Acta Cryst. (1997). A53, 537–545

Correction for Thermal Diffuse Scattering in Time-of-Flight Neutron Diffraction

N. C. POPA[a] AND B. T. M. WILLIS[b]*

[a]*Institute of Physics and Technology of Materials, PO Box MG-7, Bucharest, Romania, and* [b]*Chemical Crystallography Laboratory, University of Oxford, 9 Parks Road, Oxford OX1 3PD, England. E-mail: bertram.willis@chemcryst.ox.ac.uk*

(*Received 18 July 1996; accepted 1 March 1997*)

Abstract

A fast numerical algorithm is presented for calculating the TDS correction to Bragg peaks recorded in time-of-flight neutron diffraction studies on single crystals. The algorithm allows two average sound velocities, together with the structural parameters, to be treated as free parameters in a refinement program. The correction does not require, therefore, a prior knowledge of the elastic constants of the sample. The model is tested on a simulated set of reflection data.

1. Introduction

In any X-ray or neutron diffraction experiment, in which the aim is to determine the structure of a crystalline sample, some parasitic scattering is measured together with the Bragg scattering. Some of the parasitic scattering can be subtracted as background, but this is not the case for the scattering by acoustic phonons (*i.e.* thermal diffuse scattering, TDS). The TDS scattering is situated just under the Bragg peak and only a part of it may be subtracted. It can be reduced by making measurements at low temperature but the simplest procedure is to calculate the TDS contribution using the known elastic constants of the crystal. The first such calculation was made many years ago by Nilsson (1957) for X-ray diffraction, assuming an ω scan and an infinite slit height at the detector. Later, other authors improved the Nilsson correction; for example, Cooper & Rouse (1968) considered a finite slit height and also the case of an ω–2θ scan. For neutron diffraction, the TDS correction is more complicated than for X-rays, depending on the ratio β of the sound velocity in the crystal to the neutron velocity. In the case of the angular dispersive method of neutron diffraction, the correction is similar to that for X-rays if $\beta \leq 1$, but is different for $\beta > 1$ because TDS is then forbidden in certain regions of reciprocal space (Wllis, 1970; Cooper, 1971). The TDS correction also depends on β in wavelength-dispersive (time-of-flight) neutron diffraction but here the value of β, for which the forbidden regions exist, in turn depends on the ratio ξ between the sample-to-detector flight path and the total flight path (Willis, 1986; Popa, 1987*a*). In a recent paper by Popa & Willis (1994) [referred to below as PW1], many aspects of TDS in time-of-flight (TOF) diffractometry have been clarified and an analytical formula for the corresponding differential scattering cross section has been derived. This calculation was based on a model using two sound velocities, representing the velocities (averaged over all directions) of the longitudinal and transverse modes of vibration. Starting with this cross section, we shall calculate in the present paper the TDS correction of the Bragg peaks, as measured by TOF single-crystal diffractometry. A fast numerical algorithm is used, in which the two sound velocities, together with the structural parameters, are treated as free parameters in a refinement program. Thus, the TDS correction does not require any prior knowledge of the elastic constants. Our model is tested on a simulated set of reflection data.

For polycrystals, a numerical algorithm for the TDS correction of time-of-flight diffraction patterns has been described by Cole & Windsor (1980). They used the same two-velocities model as in the present paper. More recently, Wilson (1995) proposed an empirical method, independent of any model, to subtract the TDS contribution in time-of-flight diffractometry. The method depends on the observation that the TDS is separated from the Bragg scattering at points sufficiently far from the Bragg peak. Wilson used Gaussians to represent the two distributions and yet the TDS is often strongly asymmetrical. We believe that the direct calculation of TDS remains the safest way of correcting the diffraction peaks.

2. Integration window and general expression for the TDS correction

The integrated intensity of the diffraction peak can be written as $\mathfrak{I} = \mathfrak{I}_B + \mathfrak{I}_T = \mathfrak{I}_B(1+\alpha)$, where the suffixes B and T denote Bragg and TDS and the ratio α $(= \mathfrak{I}_T/\mathfrak{I}_B)$ is the correction that we want to calculate.

Let us suppose that the TOF diffractometer is equipped with a position-sensitive detector and denote by t the time of flight and by u and v the coordinates on the detector surface in and normal to the diffraction plane, respectively. Let us delimit on this surface a rectangular area of dimensions $(2u_0, 2v_0)$, centred on the Bragg peak position (u_B, v_B), which is large enough to include all Bragg scattered neutrons. Denoting by $I(t, u, v)$ the count rate in a given time–position channel, we form the following sums:

$$I(t,u)=\sum_{v=v_B-v_0}^{v_B+v_0} I(t,u,v); \quad I(t)=\sum_{u_B-u_0}^{u_B+u_0} I(t,u). \tag{1a, 1b}$$

$I(t)$ is the total intensity measured in the time channel t. The measurements are made between the time limits $t_B - t_b$ and $t_B + t_b$, where t_B is the time at the maximum of the Bragg peak. Following a procedure such as that used by Lehmann & Larsen (1974) to determine appropriate values of t_a and t_b, the integrated intensity of the measured diffraction peak is then

$$\mathfrak{I}=\sum_{t_B-t_b}^{t_B+t_a} I(t)-\{[(t_b+t_a)/2][I(t_B-t_b)+I(t_B+t_a)]\}. \tag{2}$$

The term in square brackets in (2) is just the uniform background obtained by fitting a straight line to the background recorded at t_a and t_b.

The sequence of operations given above to extract the background and to obtain the integrated intensity is not unique. This sequence could be changed to subtract the background from a one-dimensional distribution $I(u)$ or $I(v)$, or from a two-dimensional distribution, *e.g.* $I(t, u)$. Obviously, the TDS correction depends on the shape and volume of the three-dimensional window in the space of measurement (in our case, the time of flight and the point on the detector) in which the integrated intensity is determined. We have chosen as window a rectangular parallelepiped, using the sequence of operations (1) and (2) to arrive at a unique algorithm for the TDS correction, which is independent of the detector type. Indeed, if the detector is position sensitive only in the cordinate u or is not position sensitive at all, the measured intensity is (1*a*) or (1*b*), respectively.

Once the window and the sequence of operations have been chosen, we proceed to calculate the integrated intensity for Bragg and TD scattering. The intensity is obtained rigorously by convoluting the corresponding differential cross section with the instrumental resolution. However, this complicates our task considerably and gives little overall benefit, as the error in α introduced by ignoring resolution is smaller than the error given by using a model that assumes that all the acoustic modes propagate isotropically. If resolution is ignored, the integration is carried out directly on the differential cross sections for Bragg and TD scattering. In PWl, the TDS differential cross section was derived in terms of the variables y, γ, δ defined as

$$y=(t_B-t)/t_B; \quad \gamma=2\theta-2\theta_B=(u-u_B)/L_2;$$
$$\delta=(v-v_B)/L_2,$$

where 2θ is the scattering angle (*i.e.* the angle between the incident and scattered neutrons), θ_B is the Bragg angle and L_2 is the distance from sample to detector. This cross section is

$$(\mathrm{d}\sigma/\mathrm{d}\Omega)_{\mathrm{TDS}}=(4\pi/3)(V/v_c)F^2\sin^2\theta_B(K_BT/M_c)\times\sum_{j=1}^{2}(j/c_j^2)S_j(y,\gamma,\delta),$$

where v_c, M_c are the volume and mass of the unit cell, V the sample volume, F the structure factor for Bragg scattering, K_B the Bolzmann constant and T the temperature. The sound velocity in the crystal is c_j with $j = 1$ for the longitudinal velocity and $j = 2$ for the transverse velocity. The function $S_j(y, \gamma, \delta)$ will be discussed later. Denoting by $(y_a+y_b, 2\gamma_0, 2\delta_0)$ the dimensions of the window in the space (y, γ, δ) corresponding to $(t_a+t_b, 2u_0, 2v_0)$, and using (1) and (2), we obtain for the TDS correction:

$$\alpha=(8\pi/3)(v_c/\lambda_B^3)\sin^4\theta_B\sum_{j=1}^{2}j(K_BT/M_cc_j^2)\times\tau_j(y_a,y_b,\gamma_0,\delta_0). \tag{3}$$

Here λ_B is the Bragg wavelength and the factor τ has the following form [taking into account that $S(-y) = S(y)$]:

$$\tau=S_a+S_b-(1/2)(y_a+y_b)[S(y_a)+S(y_b)],$$

where

$$S_k=\int_0^{y_k}S(y)\,\mathrm{d}y \quad (k=a,b) \tag{4}$$

$$S(y)=\int_{-\gamma_0}^{\gamma_0}S(y,\gamma)\,\mathrm{d}\gamma \tag{5}$$

$$S(y,\gamma)=\int_{-\delta_0}^{\delta_0}S(y,\gamma,\delta)\,\mathrm{d}\delta.$$

Hence the problem reduces to the calculation of some twofold and threefold integrals of the function $S(y, \gamma, \delta)$. The integration over δ can be performed analytically but the remaining integrations can only be carried out numerically. A straightforward numerical integration is not possible because the integrand is not defined anywhere, is not continuous, and even has singularities. To obtain a correct and fast numerical algorithm, the technique of isolating singularities is necessary.

3. The distribution $S(y, \gamma, \delta)$

In PW1, we have deduced that

$$S(y,\gamma,\delta) = \begin{cases} 1/(\pi N^2) & \text{for } \beta \le \beta_\nu \\ \beta|M|/(\pi N^2 \Delta^{1/2}) & \text{for } \beta > \beta_\nu, \end{cases}$$

where

$$N^2(y,\gamma,\delta) = A^2(y,\gamma) + \delta^2 = (\gamma + y\sin 2\theta_B)^2 + 4y^2\sin^4\theta_B + \delta^2, \quad (6)$$

$$M(y,\gamma) = 2(\eta - \cos^2\theta_B)y - \zeta\gamma$$

and

$$\Delta(y,\gamma,\delta) = \beta^2 M^2 - (\beta^2\nu^2 - 1)N^2 = (1-\beta^2\eta^2)\gamma^2 + 4\sin^2\theta_B(1-\beta^2\cos^2\theta_B)y^2 - 2\sin 2\theta_B(\beta^2\eta - 1)\gamma y - (\beta^2\nu^2 - 1)\delta^2.$$

The constants η, ζ and ν are functions of the diffractometer setting (ξ, θ_B), where θ_B is the Bragg angle and ξ is the ratio of the sample-to-detector flight path to the total flight path:

$$\eta = 1 - 2\xi\sin^2\theta_B; \quad \zeta = \xi\sin 2\theta_B; \quad \nu^2 = \eta^2 + \zeta^2.$$

Three specific values of the parameter β were considered in PW1:

$$\beta_\nu = 1/\nu; \quad \beta_\eta = 1/|\eta|; \quad \beta_\theta = 1/\cos\theta_B.$$

For $\beta \le \beta_\nu$, the function $S(y, \gamma, \delta)$ is defined in any point of reciprocal space, except at the origin (the end of the Bragg wave vector), where it has an infinite singularity. For $\beta > \beta_\nu$, this function is defined only inside the surface $\Delta(y, \gamma, \delta) = 0$ and is singular on this surface. The surface is a cone of two sheets with the axis of the cone in the plane (y, γ). At $\beta = \beta_\nu$, the cone axis is normal to the line $M = 0$ and the cone angle is π. When β increases to infinity, the cone angle decreases to zero and the cone axis rotates, its slope becoming $-(\sin 2\theta_B)/\eta$. The evolution with β of the cone geometry then depends on the diffractometer setting.

The area encompassed by the ranges $\langle 0 < \theta_B < \pi/2\rangle$ and $\langle 0 < \xi < 1\rangle$ is divided into five parts (denoted in Fig. 1 by $A, \ldots, E$) by the following four curves:

$$\xi_1(\theta_B) = 1/2; \quad \xi_2(\theta_B) = 1/(2\sin^2\theta_B); \quad \xi_3(\theta_B) = 1/[4\cos^2(\theta_B/2)]; \quad \xi_4(\theta_B) = 1/[4\sin^2(\theta_B/2)].$$

On the first curve, the slope of the line $M(y, \gamma) = 0$ is zero, on the second curve $\eta = 0$ and on the third and fourth $\beta_\theta = \beta_\eta$. For the majority of TOF diffractometers, the point (θ_B, ξ) is in region A, where the path-length ratio ξ is 0.25 at zero Bragg angle and increases to 0.5 at a Bragg angle of 90°. The TDS correction for this case only will be calculated in this paper. In A, the slope of the line $M = 0$ is positive, $\eta > 0$ and $\beta_\theta > \beta_\eta$. In Fig. 2, the thick curves show the cross section of the cone in a plane parallel to the (y, γ) plane and at a given value of δ for the three significant ranges of β: $\beta_\nu < \beta < \beta_\eta$, $\beta_\eta < \beta < \beta_\theta$ and $\beta_\theta < \beta < \infty$. This is a two-branch hyperbola that degenerates into its asymptotic lines (thin lines) if $\delta = 0$. The points in the plane inside the cone, where $S(y, \gamma, \delta)$ is defined, are those outside the branches. Let us denote this domain by $D(\delta)$. The explicit expressions of the hyperbola delimiting $D(\delta)$ are the two roots of the equation $\Delta(y, \gamma, \delta) = 0$; we denote these roots by $\gamma_+(y, \delta)$ and $\gamma_-(y, \delta)$ if the equation above is solved in the variable γ or, alternatively, by $y_+(\gamma, \delta)$ and $y_-(\gamma, \delta)$ if the equation is in the variable y. These roots are given in Appendix A. They are all valid for any diffractometer setting, but Fig. 2 is different for the regions B, C, D, E. For example, in D, the slope of the line $M = 0$ is negative, $\eta < 0$ and $\beta_\theta < \beta_\eta$, and so the cross section of the cone from Fig. 2(*c*) will lie, for $\beta > \beta_\eta$, in the quadrants 1 and 3 in place of 2 and 4.

4. The distribution $S(y, \gamma)$

Now we can proceed to integrate $S(y, \gamma, \delta)$ over δ to obtain $S(y, \gamma)$. Standard tables of integrals give

$$\int dx/(a^2 + x^2) = a^{-1}\arctan(x/a) \quad (7a)$$

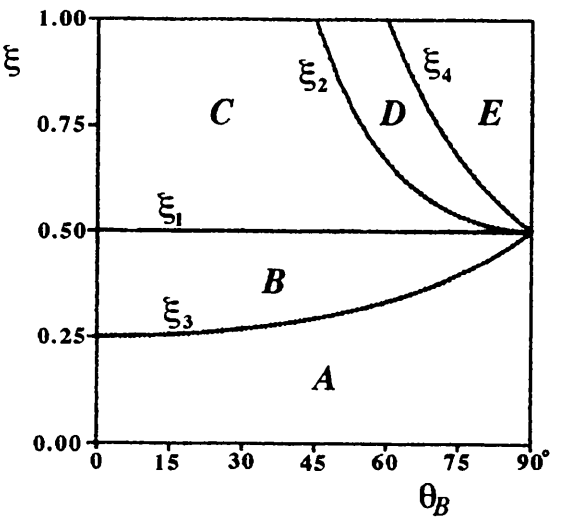

Fig. 1. Different regions (A, B, C, D, E) of the diffractometer setting (θ_B, ξ) for $\beta > \beta_\nu$. θ_B is the Bragg angle and ξ is the path-length ratio.

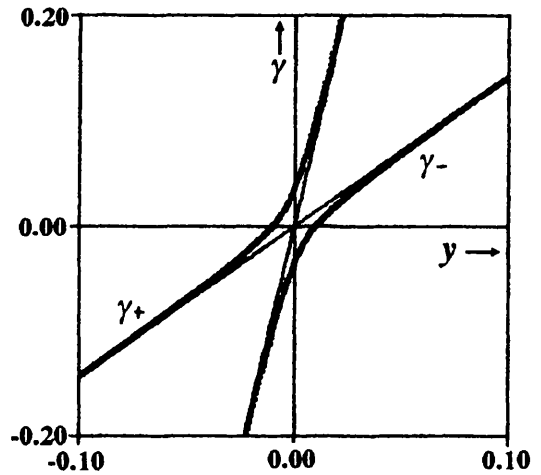

(a)

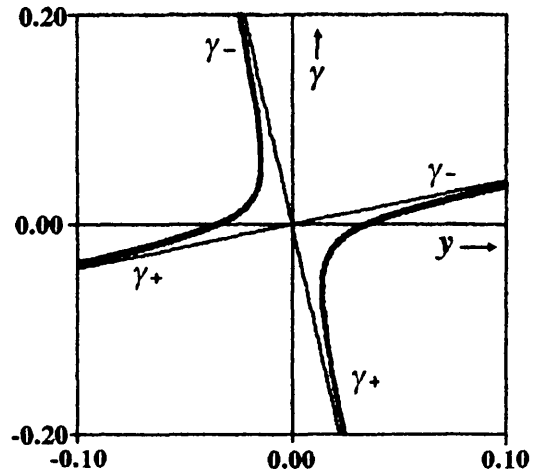

(b)

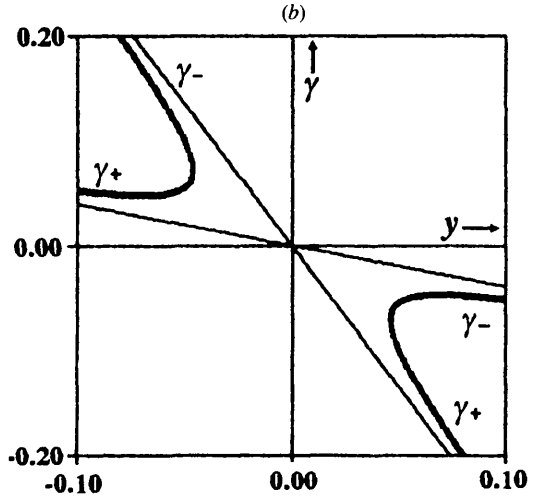

(c)

Fig. 2. The curves refer to three ranges of β: (a) $\beta_\nu < \beta < \beta_\eta$; (b) $\beta_\eta < \beta < \beta_\theta$; (c) $\beta_\theta < \beta < \infty$. [For $\beta > \beta_\nu$, the function $S(y, \gamma, \delta)$ is only defined inside a cone of two sheets.] The thick curves show the cross section of the cone with the plane δ = constant and the thin curves the cross section with $\delta = 0$. The diffractometer setting is in region A of Fig. 1.

$$\int dx/[(a^2 + x^2)(b^2 - x^2)^{1/2}] = a^{-1}(a^2 + b^2)^{-1/2} \times \arctan[xa^{-1}(a^2 + b^2)^{1/2}(b^2 - x^2)^{-1/2}]. \quad (7b)$$

Using (7a) for $\beta \leq \beta_\nu$ with $a = A$ and the limits $\pm\delta_0$, we obtain

$$S(y, \gamma) = A^{-1}(2/\pi) \arctan(\delta_0/A),$$

where A is given by (6):

$$A^2(y, \gamma) = (\gamma + y \sin 2\theta_B)^2 + 4y^2 \sin^4\theta_B.$$

For $\beta \geq \beta_\nu$, we use (7b) with $a = A$ and $b^2 = [\Delta/(\beta^2\nu^2 - 1)] + \delta^2$, but for the limits we take $\pm\min(b, \delta_0)$ in place of $\pm\delta_0$ because $S(y, \gamma, \delta)$ is defined only inside the cone discussed above. $\min(b, \delta_0)$ is δ_0 when (y, γ) lies in the domain $D(\delta_0)$ and is b when (y, γ) is in $D(0) - D(\delta_0)$. After some algebraic manipulation, the distribution $S(y, \gamma)$ is given by

$$S(y, \gamma) = \begin{cases} A^{-1}(2/\pi) \arctan(\delta_0\beta|M|A^{-1}\Delta^{-1/2}) & \\ \qquad\qquad \text{for } (y, \gamma) \subset D(\delta_0) & \\ A^{-1} \qquad \text{for } (y, \gamma) \subset D(0) - D(\delta_0) & \\ 0 \qquad\quad \text{otherwise.} & \end{cases}$$

Here Δ is calculated for $\delta = \delta_0$. $S(y, \gamma)$ has an infinite singularity at the point (0, 0). For $\beta > \beta_\nu$, it is defined only in the domain $D(0)$, having a discontinuity in the derivative on the contour of $D(\delta_0)$. If δ_0 is infinite, $S(y, \gamma)$ becomes A^{-1} for any value of β. This suggests that $S(y, \gamma)$ can be written as the difference of two functions:

$$S(y, \gamma) = S_\infty(y, \gamma) - S_\delta(y, \gamma),$$

where

$$S_\infty(y, \gamma) = A^{-1}$$

and

$$S_\delta(y, \gamma) = \begin{cases} A^{-1}[1 - (2/\pi) \arctan(\delta_0/A)] & \\ \qquad\qquad \text{for } \beta \leq \beta_\nu & \\ A^{-1}[1 - (2/\pi) & \\ \quad \times \arctan(\delta_0\beta|M|A^{-1}\Delta^{-1/2})] & \\ \qquad\qquad \text{for } \beta > \beta_\nu. & \end{cases}$$

Both $S_\infty(y, \gamma)$ and $S_\delta(y, \gamma)$ are defined everywhere for $\beta \leq \beta_\nu$, but only in the respective domains $D(0)$ and $D(\delta_0)$ for $\beta > \beta_\nu$. They are continuous except for $S_\infty(y, \gamma)$ at the point (0, 0), where it has an infinite discontinuity. At this point, $S_\delta(y, \gamma)$ has the value $2/\delta_0$ if $\beta \leq \beta_\nu$; for $\beta > \beta_\nu$, $S_\delta(y, \gamma)$ is zero on the contour of $D(\delta_0)$. The splitting of $S(y, \gamma)$ into the two components allows $S_\delta(y, \gamma)$ to be integrated numerically, having no singular point. $S_\infty(y, \gamma)$ can be integrated analytically

in the variable δ. For a certain range of β, the resulting function $S_\infty(y)$ is singular at $y = 0$, like $\ln(y)$. Isolating this singularity means that the numerical integration in y is readily performed.

5. $S(y)$ and S_k for diffractometer setting A

The use of (5) to calculate $S(y)$ from $S(y, \gamma)$ is correct only for $\beta \leq \beta_\nu$. For $\beta > \beta_\nu$, one or both integration limits $\pm\gamma_0$ must be changed at the domain borders of $S(y, \gamma)$. At the points y where the limits change, the first derivative of $S(y)$ is not continuous. As $S_\infty(y, \gamma)$ and $S_\delta(y, \gamma)$ are defined on different domains, these points are different for $S_\infty(y)$ and $S_\delta(y)$.

For $S_\infty(y)$, there are two discontinuity points, y_{10} and y_{20} (only the positive y axis is considered), and for the diffractometer setting in A these are given by

$$y_{10} = |y_-(\gamma_0, 0)|; \quad y_{20} = |y_+(\gamma_0, 0)|.$$

The integration of $S_\infty(y, \gamma)$ over γ is made by using the standard integral

$$\int dx/(a^2 + x^2)^{1/2} = \ln[x + (a^2 + x^2)^{1/2}]$$

with $x = \gamma + y \sin 2\theta_B$ and $a = 2y \sin^2 \theta_B$. For $\beta \leq \beta_\nu$, the resulting function is singular in $y = 0$, like $-\ln(y)$. By algebraic manipulation, such a term is isolated and the rest then raises no problem for numerical integration. For $\beta > \beta_\eta$, $S_\infty(y)$ has the remarkable behaviour of being constant in the interval $[0, y_{10}]$. Finally, $S_\infty(y)$ is zero for $y \geq y_{20}$ if $\beta > \beta_\theta$.

For $S_\delta(y)$, the situation is more complex. An analytical integration of $S_\delta(y, \gamma)$ over γ is no longer possible and $S_\delta(y)$ must be obtained by numerical integration. For $\beta > \beta_\nu$, $S_\delta(y)$ also has two points of discontinuity for the derivative:

$$y_1 = |y_-(\gamma_0, \delta_0)|; \quad y_2 = |y_+(\gamma_0, \delta_0)|$$

with the condition that $y_\pm(\gamma_0, \delta_0)$ exists. This condition is fulfilled only if $\beta \leq \beta_\delta$, where β_δ is defined by

$$\beta_\delta = \beta_\theta[1 + \sin^2 \theta_B(\gamma_0^2/\delta_0^2)]^{1/2}.$$

For $\beta \geq \beta_\delta$, the hyperbola in Fig. 2(*c*) lies under the line $\gamma = -\gamma_0$ and $S_\delta(y)$ is zero. As can be seen from Figs. 2(*b*) and (*c*), for $\beta_\eta < \beta < \beta_\delta$, $S_\delta(y)$ is also zero in the range $(0, y_*)$ [or $(0, y_1)$ if $\gamma_* \leq -\gamma_0$], where by (y_*, γ_*) we have denoted the coordinates of the point in which the condition $\gamma_-(y, \delta_0) = \gamma_+(y, \delta_0)$ is fulfilled. These coordinates are given by

$$y_* = \frac{\delta_0(\beta^2\eta^2 - 1)^{1/2}}{2 \sin^2 \theta_B}; \quad \gamma_* = -\frac{\delta_0(\beta^2\eta - 1) \cot \theta_B}{(\beta^2\eta^2 - 1)^{1/2}}.$$

Fig. 2(*a*) shows that, if the intersection of the hyperbola with the γ axis is over the line $\gamma = \gamma_0$, then $S_\delta(y)$ is also zero in the range $(0, y_1)$. This happens when $\beta_{\nu\eta} < \beta < \beta_\eta$, where $\beta_{\nu\eta}$ is defined by

$$\beta_{\nu\eta} = (\gamma_0^2 + \delta_0^2)^{1/2}/(\eta^2\gamma_0^2 + \nu^2\delta_0^2)^{1/2}.$$

We conclude that $S_\delta(y)$ has two or three points of discontinuity if $\beta > \beta_\nu$ and $y_* < y_1 < y_2$.

The explicit expressions for $S_\infty(y)$ and $S_\delta(y)$ are given in Appendix *B*. There are six and eight cases, respectively, which are distinguished from one another by the value of β. The long- and short-dashed curves in Fig. 3 show the profiles of $S_\infty(y)$ and $S_\delta(y)$ for four characteristic regions of β. The full curve is just $S(y)$.

Knowing the expressions for $S_\infty(y)$ and $S_\delta(y)$ and recalling that $\int dy \ln y = -y(1 - \ln y)$, it is straightforward to write down the explicit expressions for $S_{\infty k}$ and $S_{\delta k}$ ($k = a, b$) using (4). For economy of space, these expressions are not given here. We only specify that, if the interval $(0, y_k)$ contains points of discontinuity for $S_\infty(y)$ and $S_\delta(y)$, the numerical integration must be made separately in each continuity interval to avoid numerical errors.

6. The limiting value of β for a zero TDS correction

For $\beta > \beta_\eta$, the function $S_\infty(y)$ is constant in the interval $[0, y_{10}]$, and as a consequence there is a possible value β_m of β beyond which the TDS correction is zero. Two conditions must be fulfilled for the existence of β_m: $y_0 \leq y_{10}$ and $y_0 \leq y_*$, where $y_0 = \max(y_a, y_b)$. With

$$p = \eta(\eta\gamma_0 - y_0 \sin 2\theta_B), \quad q = \gamma_0 - y_0 \sin 2\theta_B,$$

$$n = 2y_0 \sin^2 \theta_B,$$

the first condition could be fulfilled only if $p > 0$. In this case, the condition gives

$$\beta \geq \beta_{1m} = p^{-1}\{pq + \nu^2n^2/2 + [(pq + \nu^2n^2/2)^2 - p^2(q^2 + n^2)]^{1/2}\}.$$

The second condition always gives

$$\beta \geq \beta_{2m} = \beta_\eta(1 + n^2/\delta_0^2)^{1/2}$$

and then

$$\beta_m = \max(\beta_{1m}, \beta_{2m}).$$

If $p \leq 0$, a limiting value β_m does not exist and the TDS correction must be made for any value of β.

7. The computer routine

The algorithm developed in this paper has been used in a computer subroutine (in Fortran), which needs as input data the diffractometer setting parameters, the window dimensions of the peak and two values of the sound velocity in the crystal. For these two sound velocities, the subroutine yields two output values of the parameter τ in (3). Most of the execution time is spent in evaluating the single and double integrals, for which we have employed a Gauss–Legendre method. Numerous tests have shown that four integration nodes ensure good precision for the single integrals. The relative error introduced in τ by decreasing the number of nodes from 10 to 4 was smaller than 0.3%. This maximum error occurred with β just larger than β_ν when δ_0 was taken as smaller than γ_0. The error decreases with increasing β, and is also less if $\delta_0 > \gamma_0$ (which often happens in practice). This is because the weights of $S_{\delta k}$ decrease in these cases. The small number of integration nodes makes the routine a fast one. It will be twice as fast if, in place of the flight times y_a and y_b, we take the single value $y_0 = (y_a + y_b)/2$, which is possible when y_a and y_b are close to one another. We believe that this high-speed routine can be used in least-squares programs to refine two (or one) average sound velocities when these are not known beforehand from other experiments.

The factor τ calculated with this routine is shown in Fig. 4 as a function of the parameter β when one of the input parameters is varied. In Fig. 4(*a*), y_0 was varied

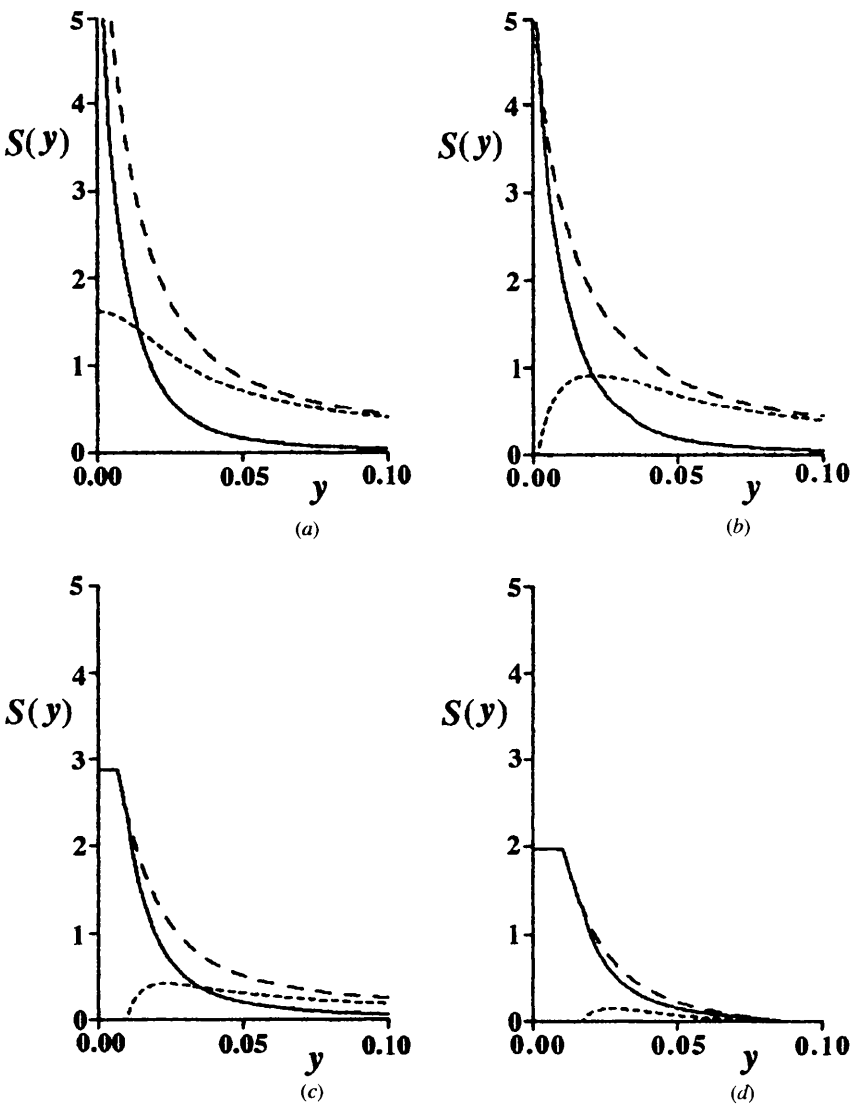

Fig. 3. The profiles $S_\infty(y)$ (long-dashed curves), $S_\delta(y)$ (short-dashed curves) and $S(y)$ [$= S_\infty(y) - S_\delta(y)$] (full curves) for $\xi = 0.2$, $\theta_B = 45°$, $\gamma_0 = 0.03$, $\delta_0 = 0.02$ and for the four characteristic ranges of β: (*a*) $\beta < \beta_\nu$; (*b*) $\beta_\nu < \beta < \beta_\eta$; (*c*) $\beta_\eta < \beta < \beta_\theta$; (*d*) $\beta_\theta < \beta < \infty$.

and, in Fig. 4(*b*), θ_B was varied. Discontinuity points in $d\tau/d\beta$ can be observed, as well as the existence, in some cases, of limiting values β_m.

8. Test of the algorithm

Using the present algorithm and a simulated set of time-of-flight reflection data, we have tested the possibility of correcting for TDS without assuming prior knowledge of the sound velocities.

A total of 103 integrated intensities of the diffraction peaks of a nickel monocrystal was generated using the values of the displacement parameter B and sound velocities c_1 and c_2 given by Cole & Windsor (1980): $B = 0.382\,\text{Å}^2$, $c_1 = 5912$ and $c_2 = 3148\,\text{m s}^{-1}$. For calculating the integration limits, $2y_0$, $2\gamma_0$ and $2\delta_0$, we used a mosaic spread of 5′ and the resolution data of the time-of-flight diffractometer DN2 installed at the pulsed reactor IBR2 in Dubna, Russia. These data were published by Popa (1987*b*) and by Balagurov, Beskrovnyi & Popa (1987). The scattering angle and flight paths were $2\theta_B = 160°$, $L_1 = 24$, $L_2 = 1$ m. For simplicity, we ignore factors common to all peaks and write the integrated Bragg intensity as $\mathfrak{I}_B = \exp[(-2B\sin^2\theta_B)/\lambda_B^2]$ and the total integrated intensity as $\mathfrak{I} = \mathfrak{I}_B[1 + \alpha(c_1, c_2)]$. We take the 'measured' integrated intensity as $\mathfrak{I}_m = \mathfrak{I} + g\sigma(\mathfrak{I})$, where $\sigma(\mathfrak{I})$ is the standard deviation and g is a random number, selected from a Gaussian distribution with a mean of zero and a dispersion of unity. A realistic standard deviation for the intensity could be $\sigma(I) = 0.01I^{1/2}$, giving a relative statistical error of 1% for the strongest peak and 3.6% for the weakest. In Fig. 5, we plot, as a function of wavelength, the integrated Bragg intensity, the integrated measured intensity and the TDS correction. As expected from (3), the correction assumes higher values at shorter wavelengths.

Parameterized models of the calculated integrated intensity $\mathfrak{I}_c$ were fitted to the measured data $\mathfrak{I}_m$ by minimizing $\chi^2 = (n_f)^{-1}\sum[\sigma(\mathfrak{I}_m)]^{-2}(\mathfrak{I}_m - \mathfrak{I}_c)^2$, where n_f is the number of degrees of freedom. The quality of fit is given by the values of the standard quantities χ^2, R and R_w. Four fits were carried out.

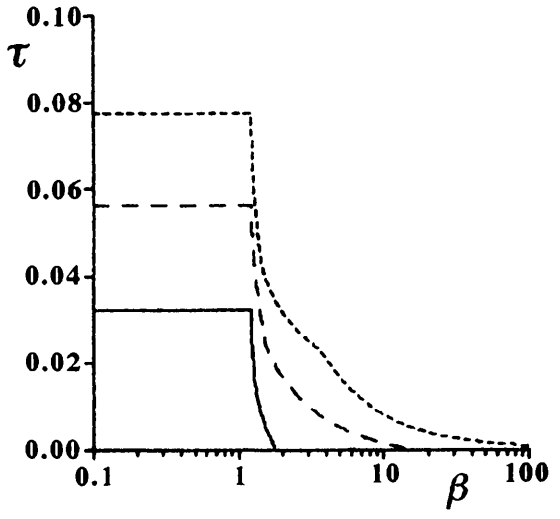

(*a*)

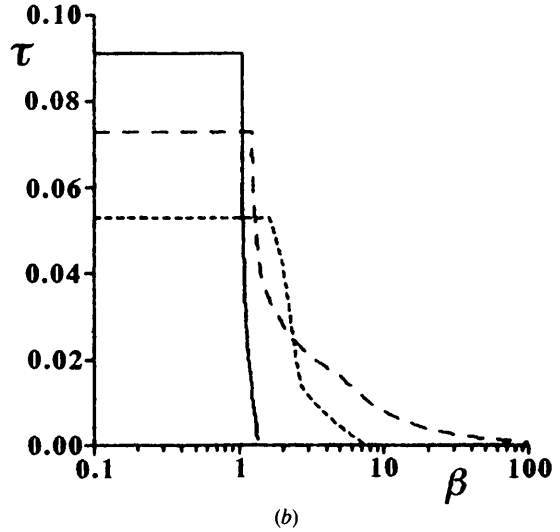

(*b*)

Fig. 4. The parameter τ as a function of β for $\xi = 0.2$, $\gamma_0 = 0.02$ and $\delta_0 = 0.03$. In (*a*), $\theta_B = 45°$ and $y_0 = 0.008$ (full curve), $y_0 = 0.015$ (long-dashed curve) and $y_0 = 0.022$ (short-dashed curve). In (*b*), $y_0 = 0.02$ and θ_B was varied: 20° (full curve), 45° (long-dashed curve) and 80° (short-dashed curve).

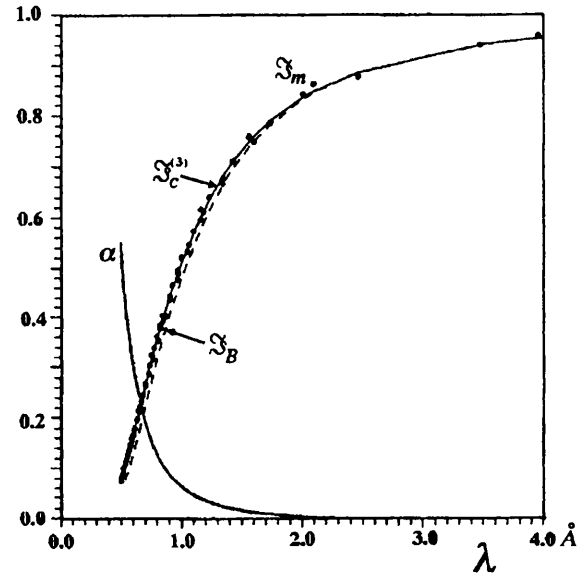

Fig. 5. TDS correction α (full curve), the integrated Bragg intensity $\mathfrak{I}_B$ (dashed curve) and the 'measured' intensity $\mathfrak{I}_m$, indicated by dots, for the simulated set of reflection data for nickel. The full curve passing through the measured points is the result of the third fit $\mathfrak{I}_c^{(3)}$.

In the first fit, TDS was ignored, so that $\mathfrak{I}_c = \mathfrak{I}_B$. The results were: $B = 0.332(1)$ Å^2, $\chi^2 = 2.88$, $R = 2.49$, $R_w = 3.05\%$. B is 13% too low and the quality of fit is poor.

The second fit was made with $\mathfrak{I}_c = \mathfrak{I}$ and TDS was included with the sound velocities, c_1 and c_2, fixed at the values given above. The results were: $B = 0.380(1)$ Å^2, $\chi^2 = 0.96$, $R = 1.32$, $R_w = 1.76\%$. There is no bias in the estimation of B and the fit is of good quality.

In the third fit, we took $\mathfrak{I}_c = \mathfrak{I}$ but with $c_1 = c_2$ as the second fitted parameter. The result of the fit was: $B = 0.380(5)$ Å^2, $c_1 = c_2 = 3.6(2) \times 10^3$ m s^{-1}, $\chi^2 = 0.97$, $R = 1.32$, $R_w = 1.76\%$. There is no bias in B and the quality of fit is the same as in the second case. The sound velocity differs by 11.5% from the weighted mean of c_1, c_2 and the curve arising from this fit is shown as $\mathfrak{I}_c^{(3)}$ in Fig. 5.

Finally, in the fourth fit, c_1 and c_2 were treated as independent fitted parameters. The result was: $B = 0.378(5)$ Å^2, $c_1 = 2.3(3) \times 10^3$, $c_2 = 8(5) \times 10^3$ m s^{-1}, $\chi^2 = 0.98$, $R = 1.32$, $R_w = 1.76\%$. The value of B and the quality of fit are as good as those from the third fit, but the two sound velocities are not well determined.

We conclude that the algorithm described above can be used successfully in calculating the TDS correction to Bragg peaks recorded by time-of-flight neutron diffraction. The algorithm allows two sound velocities (representing average longitudinal and transverse velocities), together with the structural parameters, to be treated as free parameters in a refinement program. It may turn out that an equally good refinement is obtained by using a single parameter to represent the overall sound velocity in the crystal.

APPENDIX *A*
The roots of equation $\Delta(y, \gamma, \delta) = 0$

When solved in γ, the roots are

$$\gamma_+(y,\delta) = [\sin 2\theta_B(\beta^2\eta - 1)y + P^{1/2}](1 - \beta^2\eta^2)^{-1}$$
$$\gamma_-(y,\delta) = [4\sin^2\theta_B(1 - \beta^2\cos^2\theta_B)y^2 - (\beta^2\nu^2 - 1)\delta^2] \times [\sin 2\theta_B(\beta^2\eta - 1)y + P^{1/2}]^{-1},$$

where

$$P = (\beta^2\nu^2 - 1)[4\sin^4\theta_B y^2 + (1 - \beta^2\eta^2)\delta^2].$$

Solving for y, we have

$$y_+(\gamma,\delta) = [\cos\theta_B(\beta^2\eta - 1)\gamma + Q^{1/2}] \times [2\sin\theta_B(1 - \beta^2\cos^2\theta_B)]^{-1}$$
$$y_-(\gamma,\delta) = [(1 - \beta^2\eta^2)\gamma^2 - (\beta^2\nu^2 - 1)\delta^2] \times \{2\sin\theta_B[\cos\theta_B(\beta^2\eta - 1)\gamma + Q^{1/2}]\}^{-1},$$

where

$$Q = (\beta^2\nu^2 - 1)[\sin^2\theta_B y^2 + (1 - \beta^2\cos^2\theta_B)\delta^2].$$

APPENDIX *B*
The profiles $S_\infty(y)$ and $S_\delta(y)$

We use the notation

$$R(y) = \ln\{[(\gamma_0 + y\sin 2\theta_B) + A(y,\gamma_0)]/(2\sin^2\theta_B)\}$$
$$R_1 = \ln\Big(|1 - \beta^2\eta^2|/\{[X^2 + (1 - \beta^2\eta^2)^2]^{1/2} + X\}\Big)$$
$$R_2 = \ln\Big(X/\{[X^2 + (1 - \beta^2\zeta^2)^2]^{1/2} - (1 - \beta^2\zeta^2)\}\Big),$$

where

$$X = \beta^2\eta\zeta + (\beta^2\nu^2 - 1)^{1/2}.$$

$S_\infty(y)$ is then defined differently in the six regions of the parameter β:

(i) $0 < \beta \le \beta_\nu$

$$S_\infty(y) = -2\ln y + R(y) + R(-y), \qquad 0 \le y < \infty$$

(ii) $\beta_\nu < \beta < \beta_\eta$

$$S_\infty(y) = -2\ln y + R(y) + R(-y) + R_1 + R_2, \qquad 0 \le y < y_{10}$$
$$S_\infty(y) = -\ln y + R(-y) + R_2, \qquad y_{10} \le y < y_{20}$$
$$S_\infty(y) = -2\ln y + R(y) + R(-y), \qquad y_{20} \le y < \infty$$

(iii) $\beta = \beta_\eta$

$$S_\infty(y) = -\ln y + R(-y) + R_2, \qquad 0 = y_{10} \le y < y_{20}$$
$$S_\infty(y) = -2\ln y + R(y) + R(-y), \qquad y_{20} \le y < \infty$$

(iv) $\beta_\eta < \beta < \beta_\theta$

$$S_\infty(y) = R_2 - R_1, \qquad 0 \le y < y_{10}$$
$$S_\infty(y) = -\ln y + R(-y) + R_2, \qquad y_{10} \le y < y_{20}$$
$$S_\infty(y) = -2\ln y + R(y) + R(-y), \qquad y_{20} \le y \le \infty$$

(v) $\beta = \beta_\theta$

$$S_\infty(y) = R_2 - R_1, \qquad 0 \le y < y_{10}$$
$$S_\infty(y) = -\ln y + R(-y) + R_2, \qquad y_{10} \le y < y_{20} = \infty$$

(vi) $\beta_\theta < \beta < \infty$

$$S_\infty(y) = R_2 - R_1, \qquad 0 \le y < y_{10}$$
$$S_\infty(y) = -\ln y + R(-y) + R_2, \qquad y_{10} \le y < y_{20}$$
$$S_\infty(y) = 0, \qquad y_{20} \le y < \infty.$$

The following four functions define $S_\delta(y)$ in eight ranges of β:

$$T_0(y) = \int_{-\gamma_0}^{\gamma_0} \mathrm{d}\gamma\, S_\delta(y,\gamma);$$

$$T_+(y) = \int_{\gamma_+(y,\,\delta_0)}^{\gamma_0} \mathrm{d}\gamma\, S_\delta(y,\gamma);$$

$$T_-(y) = \int_{-\gamma_0}^{\gamma_-(y,\,\delta_0)} \mathrm{d}\gamma\, S_\delta(y,\gamma);$$

$$T(y) = \int_{\gamma_+(y,\,\delta_0)}^{\gamma_-(y,\,\delta_0)} \mathrm{d}\gamma\, S_\delta(y,\gamma).$$

(i) $\beta \le \beta_\nu$

$S_\delta(y) = T_0(y), \qquad 0 \le y < \infty$

(ii) $\beta_\nu < \beta < \beta_{\nu\eta}$

$S_\delta(y) = T_+(y) + T_-(y), \qquad 0 \le y < y_1$

$S_\delta(y) = T_-(y), \qquad y_1 \le y < y_2$

$S_\delta(y) = T_0(y), \qquad y_2 \le y < \infty$

(iii) $\beta = \beta_{\nu\eta}$

$S_\delta(y) = T_-(y), \qquad 0 = y_1 \le y < y_2$

$S_\delta(y) = T_0(y), \qquad y_2 \le y < \infty$

(iv) $\beta_{\nu\eta} < \beta \le \beta_\eta$

$S_\delta(y) = 0, \qquad 0 \le y < y_1$

$S_\delta(y) = T_-(y), \qquad y_1 \le y < y_2$

$S_\delta(y) = T_0(y), \qquad y_2 \le y < \infty$

(v) $\beta_\eta < \beta < \beta_\theta$

$S_\delta(y) = 0, \qquad 0 \le y < y_*$

$S_\delta(y) = \{0; T(y)\}, \qquad y_* \le y < y_1$

$S_\delta(y) = T_-(y), \qquad y_1 \le y < y_2$

$S_\delta(y) = T_0(y), \qquad y_2 \le y < \infty$

(vi) $\beta = \beta_\theta$

$S_\delta(y) = 0, \qquad 0 \le y < y_*$

$S_\delta(y) = \{0; T(y)\}, \qquad y_* \le y < y_1$

$S_\delta(y) = T_-(y), \qquad y_1 \le y < y_2 = \infty$

(vii) $\beta_\theta < \beta < \beta_\delta$

$S_\delta(y) = 0, \qquad 0 \le y < y_*$

$S_\delta(y) = \{0; T(y)\}, \qquad y_* \le y < y_1$

$S_\delta(y) = T_-(y), \qquad y_1 \le y < y_2$

$S_\delta(y) = 0, \qquad y_2 \le y < \infty$

(viii) $\beta \ge \beta_\delta$

$S_\delta(y) = 0, \qquad 0 \le y < \infty.$

In (5) to (7), $\{0; T(y)\}$ corresponds to $\{\gamma_* \le -\gamma_0; \gamma_* > -\gamma_0\}$.

This work was supported in part by a Collaborative Research Grant awarded by NATO.

References

Balagurov, A. M., Beskrovnyi, A. I. & Popa, N. C. (1987). Communication no. P3-87-531. JINR, Dubna, Russia.

Cole, I. & Windsor, C. G. (1980). *Acta Cryst.* A**36**, 697–704.

Cooper, M. J. (1971). *Acta Cryst.* A**27**, 148–157.

Cooper, M. J. & Rouse, K. D. (1968). *Acta Cryst.* A**24**, 405–410.

Lehmann, M. S. & Larsen, F. K. (1974). *Acta Cryst.* A**30**, 580–584.

Nilsson, N. (1957). *Ark. Fys.* **12**, 247–257.

Popa, N. C. (1987*a*). Communication no. E14-87-180. JINR, Dubna, Russia.

Popa, N. C. (1987*b*). Communication no. P14-87-293. JINR, Dubna, Russia.

Popa, N. C. & Willis, B. T. M. (1994). *Acta Cryst.* A**50**, 57–63.

Willis, B. T. M. (1970). *Acta Cryst.* A**26**, 396–401.

Willis, B. T. M. (1986). *Acta Cryst.* A**42**, 514–525.

Wilson, C. C. (1995). *Nucl. Instrum. Methods*, A**354**, 38–47.